LETTERS

Structure prediction for the down state of a potassium channel voltage sensor

Michael Grabe[1]*†, Helen C. Lai[1,2]*†, Monika Jain[1], Yuh Nung Jan[1] & Lily Yeh Jan[1]

Voltage-gated potassium (Kv) channels, essential for regulating potassium uptake and cell volume in plants and electrical excitability in animals, switch between conducting and non-conducting states as a result of conformational changes in the four voltage-sensing domains (VSDs) that surround the channel pore[1]. This process, known as gating, is initiated by a cluster of positively charged residues on the fourth transmembrane segment (S4) of each VSD, which drives the VSD into a 'down state' at negative voltages and an 'up state' at more positive voltages[2]. The crystal structure of Kv1.2 probably corresponds to the up state[3], but the local environment of S4 in the down state and its motion in voltage gating remains unresolved[4–6]. Here we employed several conditional lethal/second-site suppressor yeast screens to determine the transmembrane packing of the VSD in the down state. This screen relies on the ability of KAT1, a eukaryotic Kv channel, to conduct potassium when its VSDs are in the down state, thereby rescuing potassium-transport-deficient yeast[7]. Starting with KAT1 channels bearing conditional lethal mutations, we identified second-site suppressor mutations throughout the VSD that recover yeast growth. We then constructed a down state model of the channel using six pairs of interacting residues as structural constraints and verified this model by engineering suppressor mutations on the basis of spatial considerations. A comparison of this down state model with the up state Kv1.2 structure suggests that the VSDs undergo large rearrangements during gating, whereas the S4 segment remains positioned between the central pore and the remainder of the VSD in both states.

Kv channels such as Shaker move 12–14 gating charges across the membrane on channel opening[8]—a remarkable feat because the primary role of the membrane is to form a low-dielectric barrier preventing the passage of charged species. It has been proposed that the channel accomplishes this in two ways: first, by surrounding the S4 segment, thus shielding its charges from the lipid bilayer; and second, by moving S4 a large distance through the membrane electric field[9,10]. Recently, both of these assumptions have been called into question. First, whereas mutation-intolerant patches on the periphery of the pore domain[11] indicate close apposition between the pore and VSD (as supported by cross-linking studies[12–15]), gating models developed from the X-ray crystal structures of KvAP suggest only a loose association between these domains[16]. Second, major reorientations of the VSD were revealed by cysteine accessibility experiments showing that a span of 12 S4 residues accessible to the cytoplasm in the down state becomes inaccessible in the up state[17]. Unfortunately, this result cannot discern between disparate models in which S4 moves a large distance perpendicular to the membrane (more than 15 Å; refs 5,6) or a small distance (1–2 Å; ref. 4). These studies all involve probes and linkers of dimensions comparable to the distances being measured. It is therefore desirable to develop alternative approaches to resolve these questions.

Voltage-gated ion channels are highly mobile membrane proteins that require a negative membrane potential to stabilize the down state; this poses a difficult problem for structure determination using X-ray crystallography. Here, we probe structural features of the down state using an *in vivo* yeast screen that relies on the ability of KAT1, a Kv channel from *Arabidopsis thaliana*, to rescue potassium-transporter-deficient yeast by facilitating K^+ entry into the cell. We chose to use KAT1 rather than Shaker because yeast have an extremely negative membrane potential, −100 to −250 mV (ref. 18), which drives VSDs into the down state, a state compatible with K^+ conduction for KAT1[7] but not Shaker. We first identified conditional lethal mutations in KAT1's transmembrane region that destroy the VSDs' ability to adopt the correct down state configuration compatible with channel opening, thus compromising yeast growth on low K^+ media. Next, we screened libraries of mutant VSDs to search for nearby, complementary suppressor mutations that relieve the initial strain, allowing the channel to open and rescue yeast growth. Seminal work in protein biophysics has shown that suppressor mutations most profoundly recover protein function when they lie in close proximity to the site of the original perturbation[19]. Therefore, the identified conditional lethal/second-site suppressor residues, which we call pairs, provide structural information by revealing amino acids that are likely to be in close contact in the down state. Previously, this approach was successfully used to determine the transmembrane packing of the Kir 2.1 potassium channel[20], which was later verified by the crystal structure of a bacterial homologue[21].

In an attempt to map out the packing geometry of a Kv channel in the down state, we first identified conditional lethal mutations in S1 and S4 of the VSD and S5 and S6 of the central pore. We then extensively screened these conditional lethals against three mutagenized libraries of S1–S3, S2–S4 or S4, revealing three conditional lethal/second-site suppressor pairs deep within the transmembrane region (Table 1 and Supplementary Table 1). The charge reversal mutation R171E in S4 is conditionally lethal and robustly suppressed by a corresponding charge mutation in S1, C77R (Fig. 1a). Two other pairs were identified from a screen of channels with mutagenized S2–S4, in which we intentionally introduced a conservative I94V mutation into the S1–S2 linker to aid insertion of the mutant library into KAT1 (Supplementary Discussion and Supplementary Table 2). Acidic substitutions of an invariant tryptophan (W75) in S1 compromised channel function in yeast (Fig. 1b). The suppressor M169L in S4 restores the yeast growth prevented by W75D, whereas another screen with the lethal W75E+I94V identified N99D in S2 as a second-site suppressor (Fig. 1b). Our screen also recovered two additional mutations in linker regions, L115P and Y86H + D89G, which

[1]Departments of Physiology and Biochemistry, Howard Hughes Medical Institute, and [2]Graduate Group in Biophysics, University of California, San Francisco, California 94143, USA.
†Present addresses: Department of Biological Sciences, University of Pittsburgh, Pittsburgh, Pennsylvania 15260, USA (M.G.); Center for Basic Neuroscience, University of Texas Southwestern Medical Center, Dallas, Texas 75390, USA (H.C.L.).
*These authors contributed equally to this work.

Table 1 | Identified interaction sets and exchange suppressors.

Conditional lethal mutations	Second-site suppressor mutations				
	C77R (S1)	N99D (S2)	R165K (S4)	M169L (S4)	S179N (S4)
W75D (S1)†		+	–	✓	–
W75E+I94V (S1)†		✓	ND	+	ND
R171E (S4)‡	✓	–			
R174E (S4)‡	–	–			
V204E (S5)§	–	–	–	–	✓*
H210E (S5)§	–	–	✓	✓*	–

✓, interacting pair determined from screening; +, growth on low K^+ media; –, no growth; ND, not determined. *, previously identified interactions[2]; †, ‡ and §, conditional lethal mutations in the same segment. Although M169 in S4 was identified from two different screens, M169L does not suppress V204E, and only leucine at position 169 suppresses H210E[2] or W75D (data not shown). N99D does not suppress the conditional lethal mutations in S4 or S5, thus verifying the specificity of N99D for the W75 site in S1.

suppressed W75E + I94V and R174E, respectively (Supplementary Table 1).

In addition to these three pairs in the transmembrane region, we previously discovered two pairs between S5 and S4 (Table 1)[2]. We carried out directed screens to determine whether the two pairs correspond to one S4 contacting a single S5 segment or two S5 segments of neighbouring subunits. We found that a mutation at the amino-terminal end of S4, R165K, suppresses H210E in S5 (Fig. 1a).

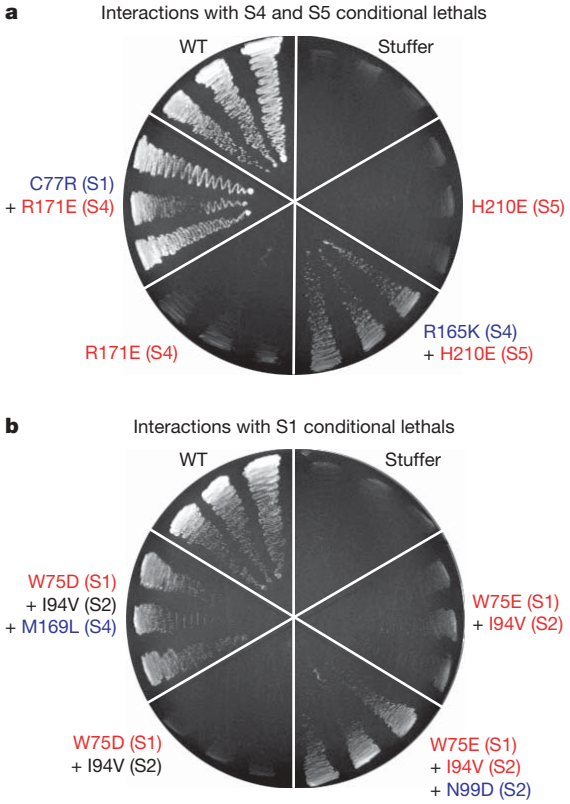

Figure 1 | Identified conditional lethal and second-site suppressor pairs. **a**, **b**, Screening revealed three pairs within the transmembrane domain of the channel from random mutagenesis and one from initial directed mutagenesis. Two pairs were identified from KAT1 conditional lethals in S4 and S5 (**a**) and two from conditional lethals in S1 (**b**). Conditional lethals (red throughout) do not support yeast growth on low potassium media (0.4 mM K^+ selective plates), whereas growth is supported by the conditional lethals with their suppressor(s) (blue throughout). The putative transmembrane segment containing the mutation is in parentheses. I94V is black with W75D because it is not required for lethality but is present during screening (see Supplementary Table 2). A KAT1 wild-type positive control and KAT1-stuffer, a non-functional negative control (see Supplementary Methods), are shown.

The physical separation of the S4 suppressors strongly supports the configuration in which S4 makes contact with two S5 segments in the down state (see Supplementary Discussion and Supplementary Fig. 1a). We also conducted control experiments by pairing each suppressor mutation with conditional lethal mutations in neighbouring segments, and we found that suppression was highly specific for the original conditional lethal site (Table 1).

We constructed a down state model of KAT1 using six of our experimentally identified interactions (ticks in Table 1) as structural constraints, in combination with bioinformatic analysis, molecular dynamics and homology modelling as described in the Methods and Supplementary Discussion. This molecular model must obey steric and secondary structural restraints. Moreover, if some of the conditional lethals were to stabilize the up state or intermediate states, rather than destabilizing the down state, it may not be possible to have a model that satisfies our hypothesis—that identified pairs represent residues in close proximity in the down state. Remarkably, a single voltage sensor resulting from this analysis accommodates the close proximity for each conditional lethal/suppressor pair (Fig. 2a). The N-terminal end of S4 contacts S5 (white), presumably of its own subunit, whereas the carboxy-terminal end contacts the S5 (grey) of the neighbouring subunit (Fig. 2). C77–R171, N99–W75, and R165–H210 are all in contact, and the distances between side chains are fairly small: M169–W75, ~2.0 Å; S179–V204, ~1.0 Å; and M169–H210, ~3.5 Å. Thus, although it is possible that the conditional lethal/second-site suppressor interactions occur in more than one state, our model is consistent with the assumption that our experiments are probing a single state of the voltage sensor.

Using the model, we computed the average distance between either of two known conditional lethals in S5—V204E and F207D—and all residues along S4 (Fig. 3a) in an attempt to engineer suppressor mutations. Two residues, S179 and F182, presented themselves as likely suppressor sites for F207D. Screening with random codons at both positions revealed that mutating S179 to histidine suppresses F207D (Fig. 3b), whereas no suppressor mutations were found for

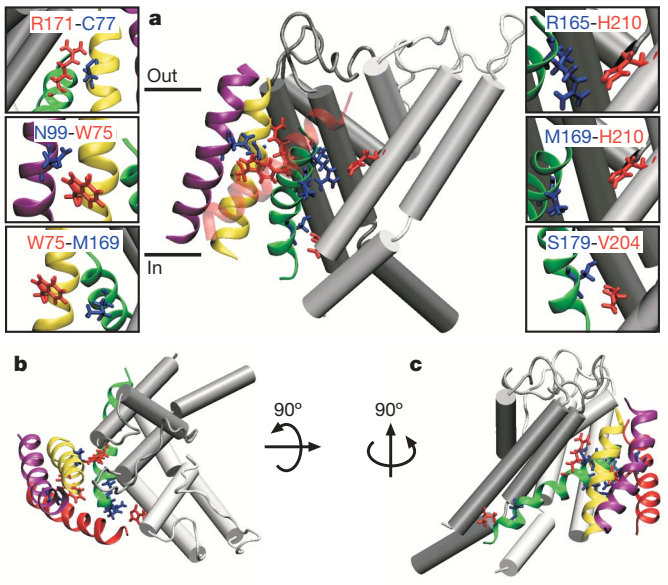

Figure 2 | A single model is consistent with the experimental data. **a**, A single VSD is pictured against two central pore subunits (white, same subunit; grey, neighbour). This is one of the top 10% of the 200 models generated as judged by the proximity of the six highlighted conditional lethal/second-site suppressor pairs. All residues are in van der Waals contact or within 1–2 Å, except M169–H210, which fall on opposing helical faces and are 3.5 Å apart. Helices are coloured: S1, yellow; S2, purple; S3, red; and S4, green. Visualization of the helical placement is aided by an extracellular view (**b**) and a rotated side view (**c**).

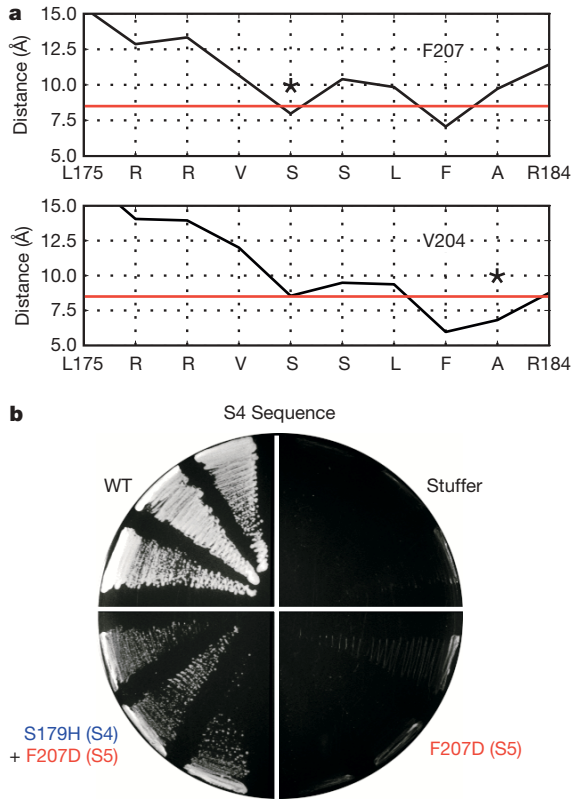

Figure 3 | Verification of the model. **a**, The average Cα to Cα distances between F207 or V204, both sites of conditional lethals, and all S4 positions were calculated for the top 10% of the models. Residues closer than 8 Å (red line) were screened against the conditional lethal mutations, V204E and F207D, to verify the model. Asterisks indicate sites of suppression. **b**, S179H, identified in **a**, rescues the conditional lethality of F207D on selective K^+ plates. Wild-type and stuffer controls are shown.

F182. Similarly, our model predicts F182 and A183 to be in close proximity to V204, and we found that polar or positively charged mutations (Ser, Asn, Lys or His) at A183 suppress V204E, whereas no suppressor at position F182 was found (data not shown). Therefore, using directed screening that was based on our model, we were able to identify suppressors with a 50% success rate compared with our initial yield of roughly one suppressor for every 10,000 attempts using random mutagenesis. Thus, these experiments provide strong evidence for the soundness of our methodology and reliability of our model.

The model reveals that S4 contacts S5 along one helical face and S1 on the N-terminal half of the opposite face, contrary to models based on KvAP, which propose that S4 has minimal contact with the rest of the channel[6]. Close proximity between S1 and S2 as well as S4 and S2 can be inferred from the shared conditional lethal mutation in S1 (W75) with suppressors in both S2 (N99D) and S4 (M169L). This positioning of S4 between the central pore and the rest of the voltage sensor may reflect energetic considerations of shielding charged residues on S4 from the bilayer[22]. Although S4 has contact with S1 and S2, the C-terminal end of the S4 helix most probably has significant lipid contact (Fig. 2c). The voltage-sensor segments (S1–S4) form a parallel bundle in the Kv1.2 structure, leaving little room for water to significantly solvate the S4 helix owing to the close, perpendicular packing. In contrast, S4 makes a 57° crossing angle with respect to S1, S2 and the pore axis in our down state model, which reduces the helix–helix packing and leaves portions of S4 exposed to the cytoplasm and extracellular space (Fig. 2 and Supplementary Fig. 2a). It is likely that water penetrates these regions, consistent with increased cysteine accessibility[17,23] and the ability of mutant VSDs to permeate ions in the down state[24,25].

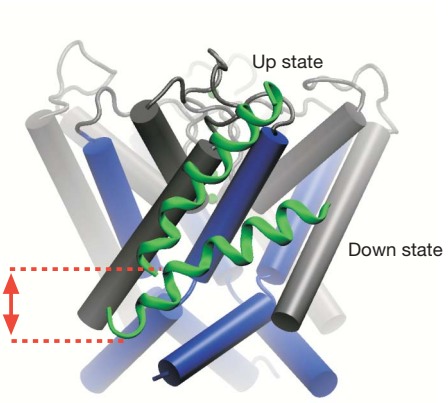

Figure 4 | The extent of S4 movement during voltage gating. The S4 segment is pictured in the down state with the up state (based on the Kv1.2 structure) superimposed. Dashed lines indicate the extent of the movement of the C-terminal end. The inner helices (S6) of the central pore are blue, and the S5 segments are grey.

Comparing our down state model with the Kv1.2 structure reveals that the N-terminal end of S4 moves 12–15 Å perpendicular to the membrane, which is in agreement with recent biotin–avidin experiments[5] (see Supplementary Movie). Electrostatic calculations using the Shaker sequence predict that this motion transfers 10–12 charges, similar to experimental measurements[8] (see Supplementary Discussion and Supplementary Fig. 2b). How does this movement gate the channel? As S4 transits to the down state, its C-terminal end descends vertically (Fig. 4), forcing the S4–S5 linker (not shown) down to a position where its interaction with the inner pore helix (S6) closes the Kv1.2 channel[26]. How can similar motions of the voltage sensors bring about the opposite gating of KAT1 (a hyperpolarization-activated channel) and Shaker (a depolarization-activated channel)? The Kv1.2 structure reveals several hydrophobic interactions between the S4–S5 linker and the S6 segment[26]; however, KAT1 is highly polar in this region, suggesting that coupling may be electrostatic (see Supplementary Discussion and Supplementary Figs 3 and 4). The voltage sensor movements suggested here should help in understanding how such fundamental differences in coupling might account for the opposite gating of hyperpolarization- and depolarization-activated channels.

METHODS

Molecular biology and library construction. Yeast screens and selection were carried out as previously described[2]. Detailed methods are described in Supplementary Information.

Model construction. We used Modeller8v0 (ref. 27) to construct an open state model of the KAT1 pore region using the Kv1.2 crystal structure. We repeated this process for the four transmembrane segments S1–S4 without the loop regions. Initial structures were generated by randomly positioning S1–S4 away from the central pore with the helices ordered as in the Kv1.2 structure. Several sets of force restraints were then placed on the initial, randomized structure, including restraints between identified pairs from our screens. Molecular dynamics simulations using NAMD 2.5 (ref. 28) were performed, allowing the protein complex to pack together. This was followed by minimization of the entire system. We repeated this process 200 times, and the model presented in the text is one of the top 10% of models ranked according to the spatial satisfaction of the experimental constraints. The orientation of S4 is very similar among the models in the top 10%.

Received 29 September; accepted 29 November 2006.
Published online 24 December 2006.

1. Hille, B. Ion channels of excitable membranes, 3rd edn (Sinauer, Sunderland, Massachusetts, 2001).
2. Lai, H. C., Grabe, M., Jan, Y. N. & Jan, L. Y. The S4 voltage sensor packs against the pore domain in the KAT1 voltage-gated potassium channel. *Neuron* **47**, 395–406 (2005).
3. Long, S. B., Campbell, E. B. & Mackinnon, R. Crystal structure of a mammalian voltage-dependent Shaker family K^+ channel. *Science* **309**, 897–903 (2005).

4. Posson, D. J., Ge, P., Miller, C., Bezanilla, F. & Selvin, P. R. Small vertical movement of a K^+ channel voltage sensor measured with luminescence energy transfer. *Nature* **436,** 848–851 (2005).
5. Ruta, V., Chen, J. & Mackinnon, R. Calibrated measurement of gating-charge arginine displacement in the KvAP voltage-dependent K^+ channel. *Cell* **123,** 463–475 (2005).
6. Jiang, Y., Ruta, V., Chen, J., Lee, A. & MacKinnon, R. The principle of gating charge movement in a voltage-dependent K^+ channel. *Nature* **423,** 42–48 (2003).
7. Anderson, J. A., Huprikar, S. S., Kochian, L. V., Lucas, W. J. & Gaber, R. F. Functional expression of a probable *Arabidopsis thaliana* potassium channel in *Saccharomyces cerevisiae*. *Proc. Natl Acad. Sci. USA* **89,** 3736–3740 (1992).
8. Schoppa, N. E., McCormack, K., Tanouye, M. A. & Sigworth, F. J. The size of gating charge in wild-type and mutant Shaker potassium channels. *Science* **255,** 1712–1715 (1992).
9. Catterall, W. A. Molecular properties of voltage-sensitive sodium channels. *Annu. Rev. Biochem.* **55,** 953–985 (1986).
10. Guy, H. R. & Seetharamulu, P. Molecular model of the action potential sodium channel. *Proc. Natl Acad. Sci. USA* **83,** 508–512 (1986).
11. Li-Smerin, Y., Hackos, D. H. & Swartz, K. J. A localized interaction surface for voltage-sensing domains on the pore domain of a K^+ channel. *Neuron* **25,** 411–423 (2000).
12. Gandhi, C. S., Clark, E., Loots, E., Pralle, A. & Isacoff, E. Y. The orientation and molecular movement of a K^+ channel voltage-sensing domain. *Neuron* **40,** 515–525 (2003).
13. Laine, M. *et al.* Atomic proximity between S4 segment and pore domain in Shaker potassium channels. *Neuron* **39,** 467–481 (2003).
14. Neale, E. J., Elliott, D. J., Hunter, M. & Sivaprasadarao, A. Evidence for intersubunit interactions between S4 and S5 transmembrane segments of the Shaker potassium channel. *J. Biol. Chem.* **278,** 29079–29085 (2003).
15. Broomand, A., Mannikko, R., Larsson, H. P. & Elinder, F. Molecular movement of the voltage sensor in a K channel. *J. Gen. Physiol.* **122,** 741–748 (2003).
16. Jiang, Y. *et al.* X-ray structure of a voltage-dependent K^+ channel. *Nature* **423,** 33–41 (2003).
17. Baker, O. S., Larsson, H. P., Mannuzzu, L. M. & Isacoff, E. Y. Three transmembrane conformations and sequence-dependent displacement of the S4 domain in Shaker K^+ channel gating. *Neuron* **20,** 1283–1294 (1998).
18. Serrano, R. & Rodriguez-Navarro, A. Ion homeostasis during salt stress in plants. *Curr. Opin. Cell Biol.* **13,** 399–404 (2001).
19. Schreiber, G. & Fersht, A. R. Energetics of protein–protein interactions: analysis of the Barnase–Barstar interface by single mutations and double mutant cycles. *J. Mol. Biol.* **248,** 478–486 (1995).
20. Minor, D. L. Jr, Masseling, S. J., Jan, Y. N. & Jan, L. Y. Transmembrane structure of an inwardly rectifying potassium channel. *Cell* **96,** 879–891 (1999).
21. Kuo, A. *et al.* Crystal structure of the potassium channel KirBac1.1 in the closed state. *Science* **300,** 1922–1926 (2003).
22. Grabe, M., Lecar, H., Jan, Y. N. & Jan, L. Y. A quantitative assessment of models for voltage-dependent gating of ion channels. *Proc. Natl Acad. Sci. USA* **101,** 17640–17645 (2004).
23. Latorre, R. *et al.* Molecular coupling between voltage sensor and pore opening in the *Arabidopsis* inward rectifier K^+ channel KAT1. *J. Gen. Physiol.* **122,** 459–469 (2003).
24. Starace, D. M. & Bezanilla, F. A proton pore in a potassium channel voltage sensor reveals a focused electric field. *Nature* **427,** 548–553 (2004).
25. Tombola, F., Pathak, M. M. & Isacoff, E. Y. Voltage-sensing arginines in a potassium channel permeate and occlude cation-selective pores. *Neuron* **45,** 379–388 (2005).
26. Long, S. B., Campbell, E. B. & Mackinnon, R. Voltage sensor of Kv1.2: structural basis of electromechanical coupling. *Science* **309,** 903–908 (2005).
27. Sali, A. & Blundell, T. L. Comparative protein modelling by satisfaction of spatial restraints. *J. Mol. Biol.* **234,** 779–815 (1993).
28. Kale, L. *et al.* NAMD2: greater scalability for parallel molecular dynamics. *J. Comput. Phys.* **151,** 283–312 (1999).

Supplementary Information is linked to the online version of the paper at www.nature.com/nature.

Acknowledgements We thank J. Schroeder for the KAT1 construct; S. Kurtz for providing the yeast strain; D. Minor for experimental guidance; W. Zhou for experimental assistance; A. Fay, F. Haass and S. Nayak for critically reading the manuscript; and members of the Jan Laboratory and B. Tu for their support, advice and input at all stages of this project. This work was supported by a National Science Foundation Interdisciplinary Informatics Fellowship (M.G.), an American Heart Association Pre-doctoral Fellowship (H.C.L.), an NIH Structural Biology Training grant (H.C.L.), and an R01 grant from the NIMH. Y.N.J. and L.Y.J. are HHMI investigators.

Author Contributions M.G. carried out all the computational aspects of this project and H.C.L. performed the yeast screens assisted by M.J. The project was a collaborative effort through iterative cycles of experiment and computational model building. All authors discussed the results and commented on the manuscript.

Author Information Reprints and permissions information is available at www.nature.com/reprints. The authors declare no competing financial interests. Correspondence and requests for materials should be addressed to L.Y.J. (lily.jan@ucsf.edu).

Supplementary Discussion

Role of I94V in conditional lethality and suppression

The relatively conservative mutation I94V was intentionally introduced into the S1-S2 linker to create a SalI cut site for inserting the S2-S4 mutant library into KAT1. We tested various combinations of single, double, and triple mutants to assess the involvement of I94V in our screens. As expected, the I94V mutation alone did not affect the channel's ability to rescue yeast (data not shown). Without the I94V mutation, W75D but not W75E compromised the ability of KAT1 channels to rescue yeast (Supplementary Table S2). A feature of the model presented in the main text is that I94V is involved in S1-S2 packing, which supports its role in creating synthetic lethality with W75E.

Subunit interactions

We wanted to determine whether the two pairs identified between S4 and S5 correspond to S4 contacting a single S5 segment or the bottom of one S5 and the top of another. The distance between S4 suppressors M169L and S179N is about 17 Å (Cα-Cα), while the distance between the corresponding conditional lethal mutations on S5, H210E and V204E, is about 9 Å within the same subunit and 29 Å between subunits. Due to the length of the side chains involved, either of these scenarios is possible, so we carried out directed screening to determine which is most likely (Supplementary Table S1D). Notably, we tested positions about one helical turn below (L172) the upper S4 suppressor, M169L, and one turn above it (R165) for their ability to suppress the conditional lethality of H210E. Screening with a randomized codon at the R165 position in S4 revealed that R165K suppressed H210E (Fig. 1b), but no such suppressor at L172 was found. The distance between S4 suppressors R165K and S179N is 24 Å supporting the configuration in which S4 makes contact with two different S5 segments in the down state.

As discussed above, we believe that S4 contacts two S5 segments from adjacent subunits. We critically probed this assumption by carrying out two sets of simulations: first, we assumed that all interactions are between the same pair of S4 and S5 segments, and second, we assumed a single S4 contacts two adjacent S5 segments (the result of these simulations is presented in the main text). Representative structures showing the S4 segment in relationship to the central pore from each set of simulations are depicted in Supplementary Fig. 1. The total Cα-Cα distance between the six restraints used in each set of simulations is similar in these models (48 Å versus 45 Å for the best two models in each set). Whereas the S4 helix remains straight when making contacts with two S5 segments (Supplementary Fig. 1a), a large helical bend (> 90°) at position L175 is necessary for spatially matching the pairs of interactions between S4 and the same S5 segment (Supplementary Fig. 1b). This bend is between charged residues R3 and R4 in Shaker-like channels according to alignment A and between R2 and R3 according to alignment B (see Supplementary Fig. 1b) —an unlikely scenario given that the leucine located at the bend in either of the alignments has the second highest helical propensity[1], and S4 is predicted to be highly helical in this region based upon several structure

prediction algorithms[2-4]. Moreover, data presented in the companion paper by Tombola and colleagues are in agreement with the configuration in panel a. Taken together, these considerations suggest that the S4 helix is largely straight in both the up and the down states.

Alignments

The alignment between S4 and S5 segments of KAT1 and Shaker/Kv1.2 is important for our analysis, and the low level of amino acid identity in this region makes aligning difficult. We present two possible alignments of S4 (Supplementary Fig. 1c): the first (A) is deduced from a massive multiple-alignment using clustal-W along with manual adjustments, and the second (B) is based on cysteine accessibility studies. Latorre and colleagues showed that R177C of KAT1 is the deepest arginine site that could be chemically modified from the external solution in the up state[5]. Similar experiments in Shaker revealed that the deepest arginine site is R368[6]. This gives strong experimental evidence for the reliability of alignment B, which we use throughout the main text. However, the conclusions of our manuscript do not depend critically on this choice.

The second question concerns the alignment of S5 segments. In our previous manuscript, we adopted an alignment of KAT1 to Shaker from Shealy *et al.*[7] that is shifted by six residues compared to the one used here (see Supplementary Fig. 1c). The Kv1.2 crystal structure revealed that this alignment provided an exceedingly short S4-S5 linker. Thus, we searched for additional evidence for an alignment. The present alignment is taken from Latorre *et al.*[8], and it has several positive features. First, the S4-S5 linker is comparable in size to the Kv1.2 linker for both S4 alignments above. Second, the extracellular end of the S5 helix of Kv1.2 terminates in a series of charged residues. The present alignment places two proline residues in KAT1 where the termination of Kv1.2 occurs, and given the role of proline residues in terminating helices this supports the present alignment. Finally, sequence analysis of 15 channels closely related to KAT1 shows that there is a sudden increase in sequence variability immediately following the second proline, P226 (data not shown). Highly variable positions often indicate water-accessibility, which would be the case if this proline marks the extracellular end of the S5 helix.

Gating charge calculations

A final test of the model is to compare the predicted voltage sensitivity with the experimentally measured values. To do this, we used Kv1.2 to model the up state of the voltage sensor and the structure suggested by our results to model the down state. While KAT1 is a hyperpolarization-activated channel and Kv1.2 is a depolarization-activated channel, gating charge movement, cysteine accessibility studies, and functional chimeric channels combining KAT1 and *Xenopus* Kv1 sequences suggest that the voltage-sensing mechanism is similar[5,6,9,10]. Homology models in both states were embedded in a low-dielectric, solute-impermeable slab mimicking the lipid environment (Supplementary Fig. 2b), and a membrane potential was imposed on the system through the far-field boundary conditions. We calculated the interaction energy of the S4 positive charges with the membrane potential, and the difference in these energies between the down and up states

to determine the gating charge transfer[11]. Carrying this out using a model of Shaker produced gating charge values of 11.0 (alignment A) or 11.6 (alignment B) using one of two very similar S4 alignments, both very close to the experimental range[12]. The robustness of this result was tested by repeating the process using another KAT1 structure randomly selected from the top 10% of the models to make homology models of Shaker in the down state. The values were 11.1 and 11.4, respectively, with the small variation due to the similarity in S4 orientation among our best models. For models based on structures in Supplementary Fig. 1b in which S4 contacts only a single S5 segment, the gating charge transfer values are 10.1 (alignment A) and 12.1 (alignment B). Both types of models in Supplementary Fig. 1 produce large gating charge values due to the large outward movement of the S4 segment. In these calculations, only the contribution due to a 17-residue span centred on the S4 helix are considered (L358-K374 for Shaker, I166-F182 for KAT1).

Repeating the process with models of KAT1 produced significantly smaller gating charge values of 5.0 (alignment A) or 7.3 (alignment B), compared to gating charge measurements of 5.2 in one study[13] and 3.0 in another[5].

The sensitivity of the Shaker channel to voltage is remarkable[14], and it is of primary interest that our model exhibits this sensitivity by producing large gating charge transfers. However, it has been shown that, of the key acidic residues in S2 (E283 and E293) and S3 (D316), neutralization of E293 but not E283 or D316 influences the gating charge[15]. To determine the contribution of these negative residues, we assessed the effect of the S2 charges, E283 and E293, on our calculations. For our Shaker models, E283 and E293 together contribute only ~0.5 charges to the total gating charge. While this is consistent with the result that E283Q has little effect on the magnitude of the gating charge, ostensibly it is at odds with the result that E293Q, 2 helical turns down from E283, reduces the gating charge by 6.3 charges per channel[15], or 1.6 charges per subunit. Clearly this latter result cannot solely be interpreted in terms of the motion of E293 through the membrane electric field, since this value cannot physically exceed unity. One possible explanation is that the lack of a charge at E293 energetically biases the conformation of the voltage sensor so that it does not undergo its full range of motion under the applied membrane potential and hence, the gating charge is greatly reduced. While this is speculative, a detailed energetic analysis of how each residue contributes to the total gating charge is needed to determine if this can explain the discrepancy between the current theoretical analysis and experiment.

Coupling voltage sensor movements to channel gating

Whereas the hydrophobic interactions between the S4-S5 linker and S6 in Kv1.2 suggest that the cytoplasmic extension of the voltage sensor segment S4 and the pore-lining helix S6 remain associated in both open and closed Kv1.2 channels, a model of the KAT1 S4-S5 linker and the S6 cytoplasmic extension based on the Kv1.2 structure places arginines from both segments in close apposition (Supplementary Fig. 3). Such a configuration is unlikely to be realized. Rather, when the S4-S5 linker is in the up state, electrostatic repulsion between S6 and the linker may induce dissociation of these regions leading to channel closure.

To assess the possible interactions between S6 and the S4-S5 linker when the VSD is in the down state, we used Modeller[16] to introduce the S4-S5 linker to the down state KAT1 transmembrane structure that we constructed from our experimental constraints. We imposed alpha-helical restraints on the linker from L185 to C198. The model presented in Supplementary Fig. 3 shows that two arginines (R190 and R197) on the S4-S5 linker, which point toward S6 in the up state according to the Kv1.2 structure, are pointing away in the down state. Meanwhile, this rotation of the linker places an aspartate (D188) close to R310 on S6. While this model lacks experimental restraints and is therefore tentative, such favourable electrostatic interactions may cause an outward motion of the C-terminus of S6 toward the S4-S5 linker and open the channel.

Our model for the gating of hyperpolarization-activated KAT1 channels based on electrostatic interactions between the S4-S5 linker and S6 is in agreement with recent experiments on spHCN channels that also activate upon hyperpolarization[17]. Prole and Yellen reported that crosslinking the S4-S5 linker to S6 of the spHCN channel, thereby forcing the cytoplasmic end of S6 to track the S4-S5 linker during VSD movements, converts the channel into a depolarization-activated channel[17]. It will be interesting in future studies to examine the possibility of two evolutionarily conserved mechanisms for voltage-gating: one where persistent association of S6 with the S4-S5 linker leads to channel opening as the VSD moves upward upon depolarization for depolarization-activated channels, and another where state-dependent interactions allow S6 to approach the S4-S5 linker only when VSD is in the down state thereby opening the channel upon hyperpolarization for hyperpolarization-activated channels.

Supplementary Methods

Molecular Biology and Library Construction. Yeast screens and selection were carried out as previously described, as were the construction of the S1-S3 and S4 libraries[18]. For the S2-S4 library, a SalI cut site was made at residue I94 thereby mutating this residue to valine, and a silent BamHI cut site was engineered in at residue W195. This construct gave the same phenotype as wild-type in the yeast assay (data not shown). The stuffer sequence containing the N- and C-terminus (residues 1-96 and 192-414 linked with a GGSGG sequence in between) of Kir 3.2 was inserted between the SalI-BamHI cut sites, providing a non-functional background and negative control cloning vector for library construction (KAT1-S2-S4-stuffer) in the same way the KAT1-S1-S3-stuffer and KAT1-S4-stuffer constructs were for the S1-S3 and S4 libraries as previously described[18]. The stuffer negative control shown in the figures is the KAT1-S4-stuffer. All constructs were verified by fluorescence sequencing. The error-prone PCR and library construction for the S2-S4 library were performed as previously described[18], with flanking primers containing the SalI and BamHI cut sites for proper ligation into the parent vector.
All targeted mutations were made using the QuikChange site-directed mutagenesis kit (Stratagene, LaJolla, CA). Randomized codons were created using the QuikChange kit with primers containing NNN (25% A,C,G,T at each site) yielding 64 possible codons or NN(G/C) yielding 32 possible codons and all amino acids.

Constructing the models. Modeller[16] was used to construct an open state model of the KAT1 pore region based on the Kv1.2 crystal structure[19] using the alignment in Supplementary Fig. 1c. Alignment of the S5 segment follows from the work of Latorre *et al.*[8], while the inner helix alignment was adapted from Shealy *et al.*[7]. We repeated this process for the four transmembrane segments S1-S4 ignoring the soluble loop regions. Both S1 and S3 are represented as polyalanine helices in the Kv1.2 structure, so an alignment is not possible, and the structure is used simply as a template for the secondary structure. S4 was constructed using either the A or B alignment in Supplementary Fig. 1c. These four helices were initially aligned with, and centred on, the pore axis in a manner consistent with known membrane topology. The S4 helix was then translated away from the pore domain, randomly rotated about its axis, tilted off-axis up to ±45°, and then rotated in the x-y plane about its centre. This was repeated for segments S1-S3, which were disposed around S4 in an order consistent with the helix order seen in the Kv1.2 structure.

Several sets of force restraints were then placed upon the initial, randomized structure:

1) Harmonic restraints were placed between six of the eight pairs identified in the screen and marked in Table 1, using a force constant of 4 kcal/mol/Å^2.

2) Our screen revealed no structural constraints for the S3 segment. To model this helix, an alignment of 30 homologous KAT1 channels was carried out from which we determined that several residues are strictly conserved yet others are highly variable. Forces were placed upon these residues either attracting them to the other VSD transmembrane elements or repelling them, with the notion that

high conservation designates protein-packing faces of the S3 helix[20]. Residues were designated as strictly conserved, highly conserved, or variable and force constants –0.008, -0.001, and 0.008 kcal/mol/Å^2 were placed on each, respectively. Harmonic restraints were also placed between the N-terminal end of S3 and the C-terminal end of S2 as well as the C-terminal end of S3 and the N-terminal end of S4.

3) Dihedral restraints were placed along the backbone of segments S1-S4 to maintain secondary structure during the simulations.

4) All backbone atoms of the central pore were fixed. S1-S4 side chains not involved in pair interactions were modelled as glycine.

Molecular dynamics simulations using NAMD 2.5 were performed at high temperature, 600K, for a total of 80 ps with a reduced 1.5 fs time step allowing the protein complex to pack together[21]. This was followed by minimization of the entire system. 200 simulations were carried out with different initial configurations of the helices S1-S4, and each final structure model was scored based on the Cα-Cα distance between lethal and suppressor residues. Our methodology closely follows that used by Roux[22].

Electrostatic calculations. All electrostatic calculations were carried out with the program APBS[23] using the PARSE parameter set for the protein partial charges[24]. The effect of the membrane potential and membrane was accounted for as described by Grabe and colleagues[11]. The dielectric value of the water, protein, and membrane were assigned values of 80, 10, and 2, respectively. The aqueous environment was modelled with a symmetric ionic solution of 100 mM. Numerically, the linearized Poisson-Boltzmann equation was solved with two levels of focusing with a spatial discretization of 0.6 Å per grid point at the finest level.

Supplementary Figures

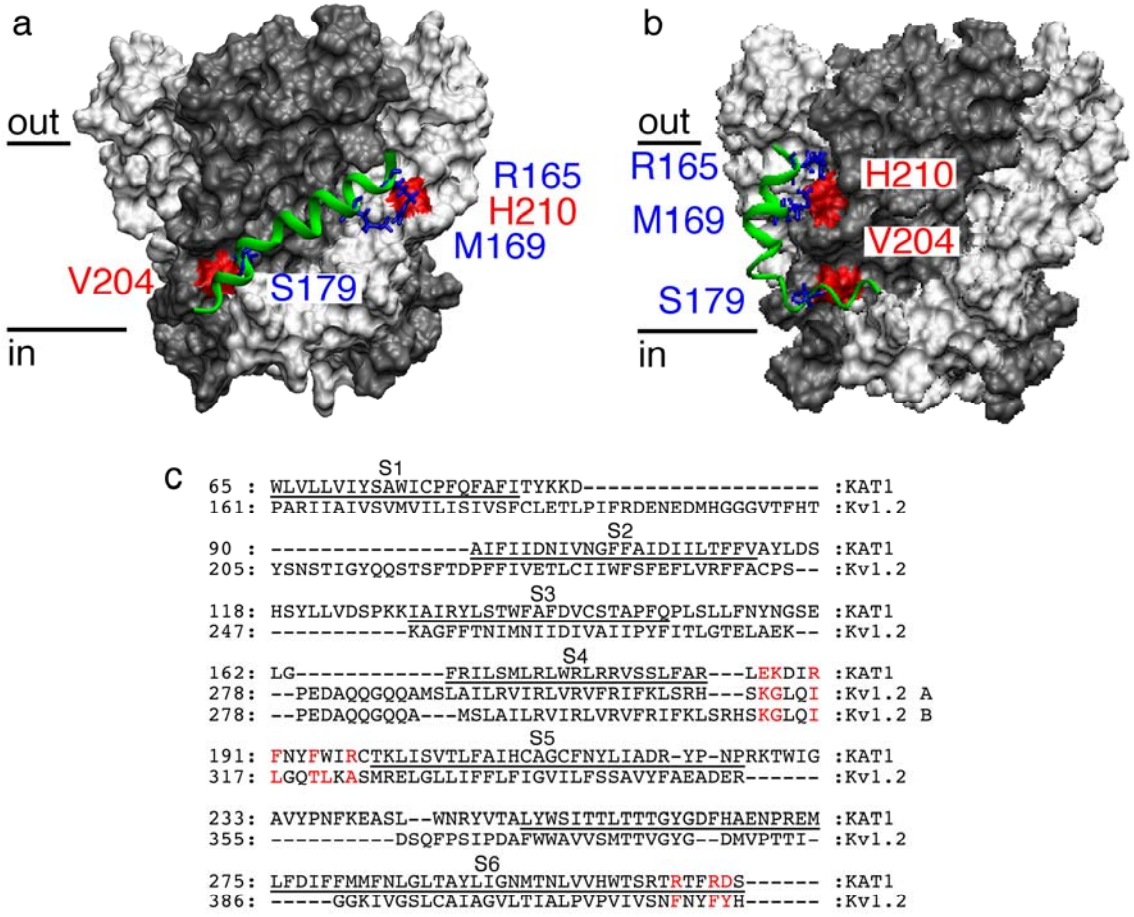

Supplementary Figure 1 | Two down state models of KAT1. Two sets of models were generated from the results of the yeast screen assuming S4 contacts a single S5 segment or two S5 segments. The central pore is shown as a surface, with alternating subunits coloured grey and white. A single, S4 segment (green) is shown in each panel. **a,** We assumed that the N-terminus of S4 contacts H210 in the white subunit and the C-terminal end contacts V204 of the neighbouring grey subunit. **b,** All interactions are between the same S4 and S5 segments. This produces a large kink in the centre of the S4 helix, but otherwise satisfies the experimental constraints quite well. **c,** The alignment of KAT1 to Kv1.2. Two possible alignments of the S4 segment are provided. Transmembrane domains are indicated above the sequence, and only underlined residues were used in constructing models. Positions coloured red indicate interacting residues between the S4-S5 linker and S6 in the Kv1.2 crystal structure[25]. Note that while many of these residues are hydrophobic in Kv1.2, they are highly charged in KAT1 suggesting that the mechanical coupling between the S4-S5 linker and the central pore may be electrostatic in KAT1 rather than hydrophobic (see Supplementary Fig. 3). Note that R294, R297, R300, and R303 in Kv1.2 are commonly referred to as R1, R2, R3, and R4, respectively.

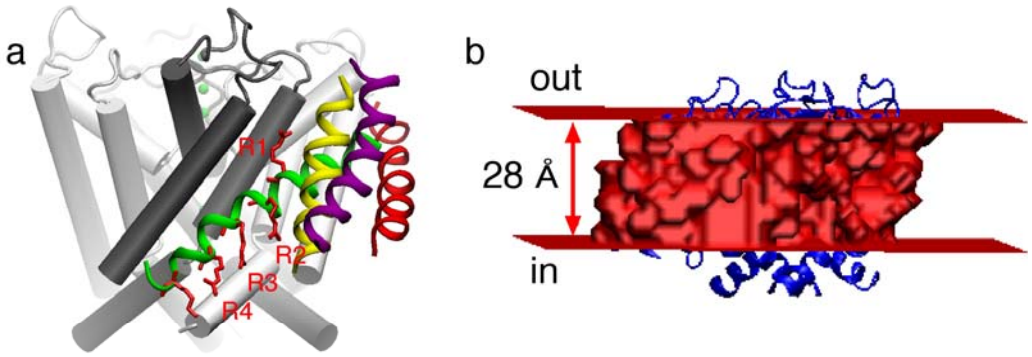

Supplementary Figure 2 | Gating charge calculations using the Shaker channel. a, Homology model of Shaker constructed on the down state model of KAT1 from Fig. 2 using alignment B from the Supplementary Discussion. The first five charged groups are represented explicitly (red sticks), and the first four are labeled R1-R4. R1 and R2 have intimate contact with S1, but the last residues point down into the cytoplasmic space. Directly behind the VSD is the neighbouring central pore subunit (grey) while its own subunit is to the right (white). **b,** The channel (blue) was embedded in a low dielectric slab (red) corresponding to the lipid bilayer, and a membrane potential was applied across the system. The slab is 28 Å thick and bounded above and below by water. Gating charge transfers were determined for the transition from the down state to the up state based on such calculations.

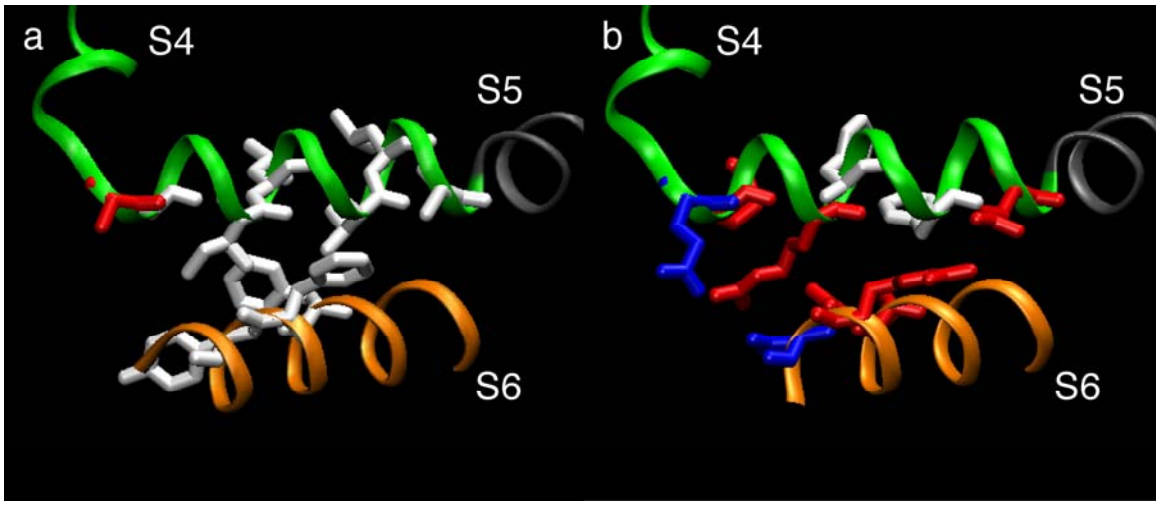

Supplementary Figure 3 | Connection between S4-S5 linker and S6. The S4-S5 linker (top, green) of Kv1.2 **(a)** and KAT1 **(b)** together with the C-terminal end of S6 (bottom, gold) are pictured looking from the cytoplasm. Kv1.2 is the crystal structure solved by Long *et al*.[19], while KAT1 is an up state model based on the Kv1.2 structure using alignment B in Supplementary Fig. 1c and constructed using Modeller[16]. Residues at the interface of S6 and the S4-S5 linker are represented explicitly. These residues are coloured red in Supplementary Fig. 1c. Acidic residues are blue, basic residues red, and neutral residues white. All white residues are hydrophobic except for the S6 residue Y417 in Kv1.2, which is polar but aromatic. Clearly, the chemistry of the Kv1.2 interface is much more hydrophobic than the KAT1 interface, which has many arginines in close proximity. When the S4-S5 linker is in the up state, the central pore of KAT1 is closed. The energetic considerations suggest that the proximity of arginines on adjacent segments of KAT1 in panel b based on the Kv1.2 structure is in fact a high energy state, implying that the open channel conformation in this KAT1 model is unrealistic, and repulsive electrostatic forces between S6 and S4-S5 linker residues will induce a closing of the central pore when the VSD is in the up state.

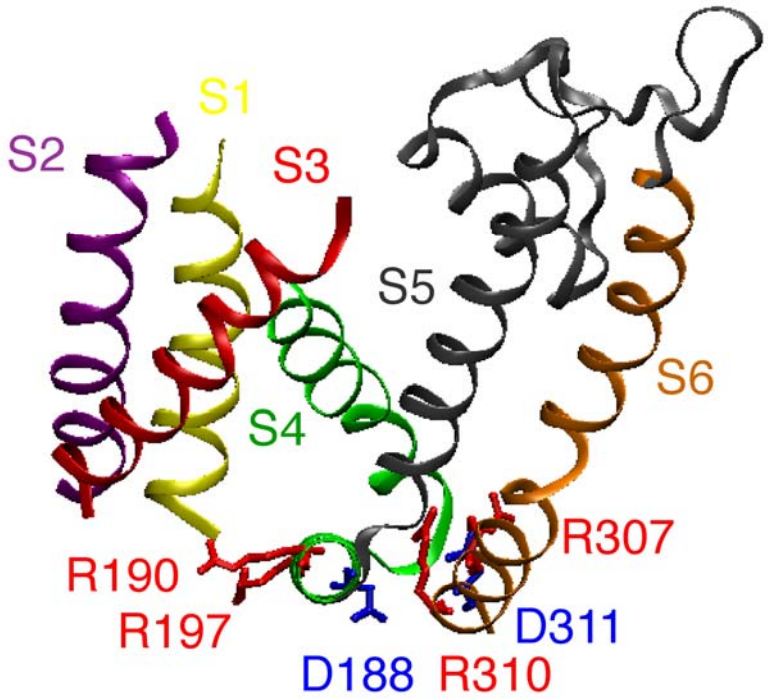

Supplementary Figure 4 | A down state model of the S4-S5 linker. The S4-S5 linker region was modelled onto the KAT1 structure in Fig. 2 using Modeller[16] with the restraint that the linker be helical. The figure is positioned as in Fig. 2a and coloured as in Supplementary Fig. 3. This view is looking down the S4-S5 linker from the membrane. Compared to Supplementary Fig. 3b, this structure represents a rotation of the arginines on the S4-S5 linker, R190 and R197, away from the interface, which may allow for favourable interactions between the C-terminus of S6, R310 and R307, with D188 on the linker. This may result in an outward radial motion of S6 leading to channel opening. This model of the linker placement lacks experimental verification, and should therefore be regarded as tentative.

Supplementary Tables

Supplementary Table 1 | Summary of screens performed to identify interactions between transmem

a, S1-S3 screen

Putative TM region of Conditional Lethal	*Conditional Lethal*	*Library Complexity*	*# Screened*	*Estimated % Rescue*	*% Unselected AA changes*	*% Unselecte b.p. change*
S4	**R171E**	1.5×10^5	9279	1.70	4.3-6	2.2-3
S4	**R174E**	1.2×10^4	10206	0.27	6-6.3	3.0
S4	**L175N**	9.4×10^3	2067	0.01	6.0	3.0
S4	**L175H**	1.6×10^4	1474	0.00	6.0	3.0
S4	**L175P**	1.1×10^4	1714	0.00	6.0	3.0
S4	**V178N**	1.7×10^4	1948	0.20	6.0	3.0
S5	**F207D**	1.8×10^4	2724	0.00	6.0	3.0
S5	**F207K**	1.0×10^3	531	0.00	6.0	3.0
S5	**F207R**	1.7×10^4	2508	0.00	6.0	3.0
S5	**F215R**	5.2×10^3	1991	0.00	6.0	3.0
S6	**N284K**	3.1×10^3	1720	0.00	6.0	3.0
S6	**N284R**	4.2×10^3	1578	0.00	6.0	3.0

b, S4 screen

Putative TM region of Conditional Lethal	*Conditional Lethal*	*Library Complexity*	*# Screened*	*Estimated % Rescue*	*% Unselected AA changes*	*% Unselecte b.p. change*
S5	**F207D**	1.2×10^3	1007	0.00	5.8	3.1
S5	**F207K**	1.4×10^3	873	0.00	5.8	3.1
S5	**F207R**	8.0×10^2	876	0.00	5.8	3.1
S5	**F215R**	5.2×10^3	4536	0.00	5.8-7.7	3.1-3.5
S6	**N284K**	1.0×10^4	2715	0.00	5.8	3.1
S6	**N284R**	1.5×10^4	2231	0.00	5.8-7.7	3.1-3.5
S6	**N284P**	1.0×10^2	548	0.00	7.7	3.5

c, S2-S4 screen

Putative TM region of Conditional Lethal	*Conditional Lethal*	*Library Complexity*	*# Screened*	*Estimated % Rescue*	*% Unselected AA changes*	*% Unselecte b.p. change*
S1	**W75E** + **I94V**	8.4×10^2	2620	0.30	5.2	2.6
S1	**W75D** + I94V	4.2×10^3	3646	0.10	5.2	2.6
S1	**W75K** + I94V	1.7×10^3	1777	0.00	5.2	2.6
S1	**W75R** + I94V	3.6×10^3	2697	0.00	5.2	2.6

d, Screens against a specific amino acid

Putative TM region of Conditional Lethal	*Conditional Lethal*	*Library Complexity*	*# Screened*	*Estimated % Rescue*	*Site of Random Mutation*	*Putative TM region of Site Random Mutation*
S4	**L175N**	960	353	0.00	V204X	S5
S4	**L175N**	1287	133	0.00	F207X	S5
S4	**L175N**	1008	176	0.00	H210X	S5
S5	**V204E**	1035	2481	0.00	R165X	S4
S5	**V204E**	1364	5223	0.00	L172X	S4
S5	**H210E**	128	2405	0.25	R165X	S4
S5	**H210E**	59	658	0.00	L172X	S4
S6	**F283P**	638	532	0.00	R165X	S4
S6	**N284K**	842	1114	0.00	M169X	S4
S6	**N284K**	1300	557	0.00	L172X	S4
S6	**N284P**	200	91	0.00	M169X	S4
S6	**N284P**	768	458	0.00	L172X	S4
S6	**N284R**	133	13*	0.00	M169X	S4

The putative transmembrane region, the conditional lethal, library complexity, number of yeast colonies screened, the estimated percent rescue, the percent amino acid (AA) changes in the unselected library, the percent base pair (b.p.) changes in the unselected library, and the suppressor mutation(s) are given. Conditional lethal mutations are in red and specific second-site suppressor mutations in blue. Screens of conditional lethal mutations against randomized regions of S1-S3 (**a**), S4 (**b**), and S2-S4 (**c**) are shown. **d,** A summary of the screens performed looking for a second-site suppressor of a particular conditional lethal at a specific site. The site of the randomized codon and its putative transmembrane segment location are given.

Supplementary Table 2 | Analysis for the requirement of the I94V mutation.

Putative TM Region	*Mutations*	*0.4 mM K+*
S1	**W75E**	+
S1 + S2	**W75E** + **I94V**	-
S1 + S2	**W75E** + **I94V** + **N99D**	+
S1	**W75D**	-
S1 + S2	**W75D** + **I94V**	-
S1 + S4	**W75D** + **M169L**	+
S1 + S2 + S4	**W75D** + **I94V** + **M169L**	+

A detailed examination of the role of the I94V mutation created by the SalI cut site for the S2-S4 mutant libraries. The phenotype in the K^+ transporter deficient yeast strain on 0.4 mM K^+ plates is represented by + for yeast growth and – for no yeast growth. W75E alone rescues yeast growth on 0.4 mM K^+ selective plates, but W75E+I94V is conditionally lethal. W75D is conditionally lethal with or without I94V. The suppressor, M169L, was discovered in conjunction with W75D+I94V; however, I94V is not required for suppression.

Supplementary Movie

A movie of the down and up gating states has been provided. The channel is viewed from the extracellular space, and subunits are coloured silver and blue, alternatively. A potassium ion (purple) can be viewed in the centre of the channel, and the central pore remains unchanged in both states since the up state is based on the open Kv1.2 channel and the down state is based on the open KAT1 channel. The VSDs undergo large rearrangements at the edge of the channel, and they are next to the pore domain of the neighbouring subunit in the up state and their own subunit in the down state.

References

1 Pace, C.N. & Scholtz, J.M. *Biophys. J.* **75,** 422-427 (1998).
2 Adamczak, R., Porollo, A., & Meller, J. *Proteins* **59,** 467-475 (2005).
3 Jones, D.T. *J. Mol. Biol.* **292,** 195-202 (1999).
4 Ouali, M. & King, R.D. *Protein Sci.* **9,** 1162-1176 (2000).
5 Latorre, R. *et al. J. Gen. Physiol.* **122,** 459-469 (2003).
6 Baker, O.S., Larsson, H.P., Mannuzzu, L.M., & Isacoff, E.Y. *Neuron* **20,** 1283-1294 (1998).
7 Shealy, R.T., Murphy, A.D., Ramarathnam, R., Jakobsson, E., & Subramaniam, S. *Biophys. J.* **84,** 2929-2942 (2003).
8 Latorre, R., Munoz, F., Gonzalez, C., & Cosmelli, D. *Mol. Membr. Biol.* **20,** 19-25 (2003).
9 Mannikko, R., Elinder, F., & Larsson, H.P. *Nature* **419,** 837-841 (2002).
10 Cao, Y., Crawford, N.M., & Schroeder, J.I. *J. Biol. Chem.* **270,** 17697-17701 (1995).

11 Grabe, M., Lecar, H., Jan, Y.N., & Jan, L.Y. *Proc. Natl. Acad. Sci. USA* **101,** 17640-17645 (2004).

12 Schoppa, N.E., McCormack, K., Tanouye, M.A., & Sigworth, F.J. *Science* **255,** 1712-1715 (1992).

13 Hoshi, T. *The Journal of general physiology* **105,** 309-328 (1995).

14 Sigworth, F.J. *Nature* **423,** 21-22 (2003).

15 Seoh, S.A., Sigg, D., Papazian, D.M., & Bezanilla, F. *Neuron* **16,** 1159-1167 (1996).

16 Sali, A. & Blundell, T.L. *J. Mol. Biol.* **234,** 779-815 (1993).

17 Prole, D.L. & Yellen, G. *J. Gen. Physiol.* **128,** 273-282 (2006).

18 Lai, H.C., Grabe, M., Jan, Y.N., & Jan, L.Y. *Neuron* **47,** 395-406 (2005).

19 Long, S.B., Campbell, E.B., & Mackinnon, R. *Science* **309,** 897-903 (2005).

20 Minor, D.L., Jr., Masseling, S.J., Jan, Y.N., & Jan, L.Y. *Cell* **96,** 879-891 (1999).

21 Kale, L. *et al. J. Comp. Phys.* **151,** 283-312 (1999).

22 Roux, B. *Novartis Found. Symp.* **245,** 84-101; discussion 101-108, 165-108 (2002).

23 Baker, N.A., Sept, D., Joseph, S., Holst, M.J., & McCammon, J.A. *Proc. Natl. Acad. Sci. USA* **98,** 10037-10041 (2001).

24 Sitkoff, D., Sharp, K.A., & Honig, B. *J. Phys. Chem.* **98,** 1978-1988 (1994).

25 Long, S.B., Campbell, E.B., & Mackinnon, R. *Science* **309,** 903-908 (2005).